Convective–Radiative-Mixing Processes in the Tropical Ocean–Atmosphere

Chung-Hsiung Sui
Institute of Hydrological and Oceanic Sciences and Department of Atmospheric Sciences, National Central University, Taoyuan, Taiwan
sui@ncu.edu.tw

Xiaofan Li
Joint Center for Satellite Data Assimilation, NESDIS, NOAA, Camp Springs, Maryland, USA

William K.-M. Lau and Wei-Kuo Tao
Laboratory for Atmospheres, Goddard Space Flight Center, Greenbelt, Maryland, USA

Ming-Dah Chou
Department of Atmospheric Sciences, National Taiwan University, Taipei, Taiwan

Ming-Jen Yang
Institute of Hydrological and Oceanic Sciences and Department of Atmospheric Sciences, National Central University, Taoyuan, Taiwan

Understanding convective–radiative-mixing processes is crucial in making better predictions about tropical climate. The cloud-resolving model and the mixed-layer model, combined with observations, are powerful tools for studying these physical processes interacting with climate. In this article, the authors' research work of the past 15 years on tropical climate processes is reviewed. The topics reviewed include climate equilibrium study, tropical convective responses to radiative and microphysical processes, the diurnal cycle, cloud clustering and associated cloud-microphysical processes, precipitation efficiency, air–sea exchanges and ocean-mixing processes at diurnal-to-intraseasonal scales, and coupled boundary layer and forced oceanic responses. Representation of these processes in climate models and future perspectives are also discussed.

1. Introduction

Clouds play an important role in regulating weather and climate in the tropical ocean–atmosphere system through convective–radiative-mixing processes. The incoming solar radiative flux and the internal climate oscillations provide the environment with a large amount of unstable energy, which initiates the formation of cloud clusters. The development of convection, in turn, significantly modifies the environment by redistributing momentum, temperature, moisture, and salinity vertically through radiative, microphysical, and dynamic mixing processes. These processes are fundamentally important in maintaining tropical oscillations and the climate state.

To improve our knowledge of the convective–radiative-mixing processes, appropriate models like cloud-resolving models are powerful tools. Soong and Ogura (1980a) performed a pioneering study using their two-dimensional slab-symmetric numerical cloud model to examine the statistical properties of cumulus clouds that respond to the given large-scale forcing, which is mainly a vertical velocity. Their nonhydrostatic model with an anelastic approximation includes prognostic equations for momentum, temperature, specific humidity, and cloud species. This model was greatly improved later at the NASA Goddard Space Flight Center (GSFC), and named the Goddard cumulus ensemble (GCE) model (Tao and Simpson, 1993; Tao, 2003; Tao *et al.*, 2003). The GCE model includes detailed solar and infrared parametrization schemes (Chou *et al.*, 1991, 1997; Chou and Suarez, 1994a), cloud-microphysical parametrization schemes for cloud water, raindrops, cloud ice, snow, and graupel (Rutledge and Hobbs, 1983, 1984; Lin *et al.*, 1983; Tao *et al.*, 1989; Krueger *et al.*, 1995), and subgrid-scale turbulence closure (Klemp and Wilhelmson, 1978).

The GCE model was originally designed to study the cumulus response to large-scale forcing (a prospective from a grid box of general circulation models), which can be imposed in the model in two ways: one with a vertical velocity and the other with heat and moisture source/sink. The model has been applied to case-oriented short-term simulations such as deep tropical cumulus clouds (Soong and Tao, 1980b), tropical squall line (Tao and Simpson, 1989), cloud interaction and merging (Tao and Simpson, 1984), and three-dimensional tropical clouds (Tao and Soong, 1986; Tao and Simpson, 1989).

In addition to the one-way response to large-scale forcing, convective–radiative processes may interact with climate change to form a feedback loop, like the feedback mechanisms of water vapor-cloud radiative forcing and surface evaporative cooling to climate warming (e.g. Newell, 1979; Fu *et al.*, 1992; Hartmann and Michelsen, 1993; Lau *et al.*, 1994a; Prabhakara *et al.*, 1993; Ramanathan and Collins, 1991; Lindzen, 2001). Some of these climate feedback mechanisms may be investigated using a cloud resolving model. Lau *et al.* (1993, 1994a) and Sui *et al.* (1994) integrated the two-dimensional GCE model imposed with the large-scale vertical velocity to reach quasi-equilibrium states, applying the cloud-resolving model as a new tool for studying the effects of the convective–radiative interaction on tropical climate.

Based on extensive knowledge acquired through previous studies, longer simulations were performed to study the cumulus ensemble response of the model to the vertical velocity derived from observational data such as Marshall Island data (Yanai *et al.*, 1973; Sui *et al.*, 1994). Other research groups employed different cloud-resolving models, and successfully simulated the deep convective response to large-scale forcing observed in the Global Atmosphere Research Programme Atlantic Tropical Experiment (GATE) (e.g. Xu and Randall, 1996; Grabowski *et al.*, 1996) and the TOGA COARE (e.g. Wu *et al.*, 1998; Li *et al.*, 1999; Johnson *et al.*, 2002).

In addition to the studies just mentioned, the GCE model has been further extended to study various convective–radiative processes related to cumulus ensemble responses to large-scale forcing (Li *et al.*, 1999, 2002b, 2005), diurnal cycle (Sui *et al.*, 1998a), microphysical processes and cloud clusters (Peng *et al.*, 2001; Li *et al.*, 2002c; Sui and Li, 2005), and precipitation efficiency (Li *et al.*, 2002a; Sui *et al.*, 2005, 2007b). Similarly, an ocean mixed layer model has been used to study air–sea exchange and ocean mixing at

diurnal to intraseasonal scales (Sui *et al.*, 1997b; Lau and Sui, 1997; Li *et al.*, 1998; Sui *et al.*, 1998b).

This article will highlight major scientific findings made by the authors during the past 15 years at NASA/GSFC, USA, and the National Central University, Taiwan. In the next section, the roles of convective–radiative processes in climate equilibrium states, cumulus ensemble responses, the diurnal cycle, microphysical processes and the development of cloud clusters, and precipitation efficiency will be reviewed. Air–sea exchange and ocean mixing at diurnal-to-intraseasonal scales will be discussed in Sec. 3. The coupled boundary layer at the atmosphere–ocean interface and forced oceanic responses will be addressed in Sec. 4. Representation of convective–radiative processes in climate models will be discussed in Sec. 5. A summary and a discussion are given in Sec. 6.

2. Convective–Radiative Processes

2.1. *Cloud-resolving modeling for climate equilibrium and feedback study*

Lau *et al.* (1993) and Sui *et al.* (1994) studied tropical water and energy cycles, and their roles in the tropical convective systems, by integrating the two-dimensional cloud-resolving model to the climate equilibrium states. The model is imposed with a time-invariant, horizontally uniform, large-scale vertical velocity and a fixed SST at 28°C, in which the simulated atmosphere is conditionally unstable below the freezing level and close to neutral above the freezing level. After the adjustment, in about 20 days, the simulations reach the quasi-equilibrium states. In the convective–radiative equilibrium conditions, two-thirds and one-third of surface rainfall come from convective and stratiform clouds, respectively. The vertically integrated moisture budget shows that three-fourths of the total moisture supply is from the moisture advection associated with the imposed large-scale vertical velocity, whereas one-third of the total moisture supply is from the surface evaporation flux. The total moisture supply is completely converted into surface rainfall. The heat budget displays that the cooling from radiation, and temperature advection associated with the imposed large-scale vertical velocity, are mainly balanced by the latent heat release associated with the precipitation processes.

Ramanathan and Collins (1991) conducted an observational analysis of measurements from NASA's Earth Radiation Budget Experiment (ERBE) during the 1987 El Niño and proposed a cirrus cloud thermostat effect. They proclaimed that cloud-radiative cooling by cirrus counteracts the super-greenhouse warming, and limits SST over the western Pacific warm pool to a rather uniform distribution between 29°C and 30°C. Lau *et al.* (1994a) further used the cloud-resolving model to assess the cirrus-cloud thermostat effect for tropical SST by analyzing the net radiation flux at the top of the atmosphere and the net heat exchanges at the ocean–atmosphere interface. The model is integrated with the SST's of 28°C and 30°C, and with and without the large-scale forcing, respectively. The net radiation flux at the top of the atmosphere comprises the net absorbed solar radiation averaged over clear sky regions, the longwave radiation emitted by the ocean surface, atmospheric greenhouse effect, and longwave and shortwave cloud forcings. The net heat flux at the ocean–atmosphere interface consists of solar and longwave radiation, sensible and latent heat fluxes. The comparison of the experiments with the same large-scale forcing

but different SST's shows that the largest changes in the components contributing to the net radiation flux at the top of atmosphere are due to the emission of the surface longwave radiation, and greenhouse warming by the increase in water vapor, which to a large degree offset each other. The magnitude of the emission of the surface longwave radiation is smaller than the greenhouse warming, suggesting no apparent "super-greenhouse" effect. The changes in longwave and shortwave cloud forcings are small, and are insensitive to the changes in the SST's, because the change in the SST induces the change in low and mid-tropospheric clouds, but does not have an impact on upper tropospheric clouds. The change in the net heat flux at the ocean–atmosphere interface is due mainly to the change in the surface latent heat flux. The increase in the SST induces surface cooling by increasing surface evaporation. The increase in the SST produces a 13% increase in surface precipitation. The comparison of the experiments with the same SST's but different large-scale forcings (with and without the forcing) shows that the largest changes in the budget at the top of the atmosphere occur in the shortwave and longwave cloud forcings, which in large part cancel each other out. The experiment without the forcing undergoes a large reduction of the greenhouse effect by decreasing the moisture. At the ocean–atmosphere interface, the largest change appears in the surface radiative flux as a result of the largest difference of clouds between the experiments with and without large-scale forcing. More discussions on the cloud-resolving modeling assessment of the cirrus cloud thermostat hypothesis can be found in Ramanathan *et al.* (1994) and Lau *et al.* (1994b).

2.2. *Cumulus ensemble responses to radiative and microphysical processes*

Li *et al.* (1999) conducted two experiments to study cloud–radiation interaction. The cloud single scattering albedo and asymmetry factor varied with clouds and environmental thermodynamic conditions in one experiment, whereas they were fixed at 0.99 and 0.843, respectively, in the other experiment. A comparison of solar radiation calculations between the two experiments showed that the experiment with the varying single scattering albedo and asymmetry factor had stronger solar radiation absorption by ice clouds in the upper troposphere than did the experiment with the constant single scattering albedo and asymmetry factor. The difference in temperatures between the two experiments further showed that the temperature around 200 mb was 2°C warmer in the experiment with the variable single scattering albedo and asymmetry factor than in the experiment with constant values.

A statistical analysis of the clouds and surface rain rates revealed that stratiform (convective) clouds contributed to 33 (67) % of the total rain in the experiment with the variable cloud optical properties and 40 (60) % in the experiment with the constant cloud optical properties. The fractional cover by stratiform clouds increased from 64% in the experiment with the variations to 70% in the experiment with the constants. These sensitivity tests show the cloud–radiation interaction processes for stabilizing the atmosphere, in which the change in the vertical heating gradient by solar radiation due to variations of cloud optical properties stabilizes the middle and upper troposphere and contributes to the reduction of stratiform clouds, which further stabilizes the cloud system by reducing infrared cloud top cooling and cloud base warming.

Li *et al.* (2005) carried out two experiments to investigate the role of precipitation–radiation interaction in thermodynamics. One experiment includes the precipitation–radiation interaction, while the other excludes it. The experiment excluding the interaction produces 1–2°C colder and 1–1.5 g kg^{-1} drier than the experiment including the interaction. The comparison of the

heat budget between the two experiments shows that the experiment excluding the interaction exhibits a more stable upper troposphere (above 500 mb) and a more unstable lower troposphere (below 500 mb) compared to the experiment including the interaction. The more stable upper troposphere suppresses the development of ice clouds that are responsible for the cooling bias, whereas more radiative cooling accounts directly for a cooling bias in the mid- and lower troposphere in the experiment excluding the interaction. The analysis of moisture budgets shows that the suppression of rain evaporation as a result of a less stable mid- and lower troposphere induces a drying bias when the experiment excludes the precipitation–radiation processes.

Cloud-microphysical processes determine conversion between environmental moisture and cloud hydrometeors. The microphysical parametrization of cloud ice and snow proposed by Hsie *et al.* (1980) was originally used in the cloud-resolving model, which produced a relatively small amount of cloud ice and snow compared to the observations. Hsie *et al.* (1980) modified the work of Orville and Kopp (1977) based on the equation of the rate of growth of ice crystals by deposition proposed by Koenig (1971), and formulated the depositional growth of cloud ice in mass and size to become snow by the mixing ratio divided by a time scale that is needed for an ice crystal to grow from a radius of 40 μm to 50 μm. Based on the aircraft observations, Krueger *et al.* (1995) suggested that the time scale in the depositional growth of snow from cloud ice should be for a crystal to grow from a radius of 40 μm to 100 μm, which increases the amount of cloud ice and snow significantly, as indicated by Li *et al.* (1999). More cloud ice leads to more infrared cooling at the cloud top, and less heating below the cloud top. Li *et al.* (1999) conducted additional experiments in which the cloud–radiation interaction is excluded, and found that the exclusion of cloud–radiation interaction and the reduction of ice clouds have a similar thermal effect, whereas the two experiments have different impacts on moisture. The simulation excluding cloud–radiation interaction causes drying by enhancing condensation, whereas the simulation with reduced ice clouds by the microphysics scheme induces moistening by suppressing condensation.

Li *et al.* (2005) further examined the role of the depositional growth of snow from cloud ice by conducting the comparison study with two experiments: one with the snow depositional growth, and the other without. The results show that the experiment without the snow depositional growth produces a much larger amount of cloud ice than the experiment with the snow depositional growth. The budget of cloud ice further reveals that the vapor deposition rate is balanced by the conversion from cloud ice to snow and the depositional growth of snow from cloud ice. When the growth of snow from cloud ice is absent, the cloud ice could be accumulated and its amount becomes anomalously large. The analysis of the heat budget indicates that the anomalous amount of cloud ice reflects a large amount of solar radiation, and the upper tropospheric atmosphere becomes anomalously cold whereas it traps a large amount of infrared radiation and the lower tropospheric atmosphere becomes anomalously warm. Thus, the depositional growth of snow from cloud ice is an important sink for cloud ice.

Tropical convection (surface rainfall) occurs as a result of instability (convective available potential energy, CAPE) in the environment. Since the environmental time scales (a few days and longer) are much longer than the convective time scales (a few hours or less), the "quasi-equilibrium" between the rate of production of available potential energy by the large-scale processes and the rate of consumption of the available potential energy by the convection is the basic assumption which Arakawa and Schubert (1974) used to develop their cumulus parametrization scheme. A decrease in the CAPE often coincides with the development

of convection so that the CAPE and rain rate are negatively correlated (e.g. Thompson *et al.*, 1979; Cheng and Yanai, 1989; Wang and Randall, 1994; Xu and Randall, 1998). The phase relation between the CAPE and rainfall is due to the coupling between the environmental dynamic and thermodynamic fields (Cheng and Yanai, 1989). The phases of the CAPE and rainfall could be different, because it takes time for clouds to develop. This phase difference can be included with relaxation of the quasi-equilibrium assumption in cumulus parametrization (e.g. Betts and Miller, 1986; Randall and Pan, 1993). The minimum CAPE typically occurs a few hours after the maximum rainfall, as indicated by the observational analysis. Xu and Randall (1998) interpreted the maximum phase lag as the adjustment time scale from disequilibrium to equilibrium states in the presence of time-varying large-scale forcing. Since the CAPE is calculated in a Lagrangian framework and the relevant equations cannot be derived, the physical processes responsible for the phase difference between the CAPE and the surface rain rate cannot be examined. However, an alternative for studying the phase difference has been developed in an Eulerian framework by Li *et al.* (2002b), in which potential and kinetic energy in an Eulerian framework represent the CAPE and surface rain rate in a Lagrangian framework, respectively.

Lorenz (1955) introduced the concept of available potential energy for a dry atmosphere that represents the portion of the potential energy that can be transferred into kinetic energy. He defined the available potential energy for a dry atmosphere as the difference between the actual total enthalpy and the minimum total enthalpy that could be achieved by rearranging the mass under adiabatic flow. The dry enthalpy per unit mass is defined as the product of the temperature and the specific heat at constant pressure. In the absence of energy sources and sinks, the total kinetic energy and total enthalpy are conserved during adiabatic expansion. In a moist atmosphere, latent heat energy should be included in the energy conservation. The latent heat energy per unit mass is defined as the product of the specific humidity and the latent heat of vaporization at 0°C. In the absence of energy sources and sinks, the total kinetic energy, enthalpy and latent heat energy are conserved during dry and subsequent saturated adiabatic expansion. Therefore, the moist available potential energy is defined as the difference between the actual moist potential energy (sum of the enthalpy and latent heat energy) and the minimum moist potential energy that could be achieved by rearranging the mass under moist adiabatic processes. Li *et al.* (2002b) derived a set of equations for conversions between the moist available potential energy and kinetic energy in an Eulerian framework. Their equations were demonstrated to be the same as those derived by Lorenz (1955) in the absence of moisture.

Lag correlation analysis by Li *et al.* (2002b) showed that the maximum perturbation kinetic energy associated with the simulated convective systems and its maximum growth rate lags and leads the maximum imposed large-scale upward motion by about 1–2 hours respectively, indicating that the convection is phase-locked with the imposed large-scale forcing. Their imposed large-scale vertical velocity had time scales longer than the diurnal cycle, whereas the simulated convective systems had an average lifetime of about 9 hours. The imposed large-scale upward motion decreases the horizontal-mean moist available potential energy by the associated vertical advective cooling, providing a favorable environment for the development of convection.

They further showed that the maximum latent heating and vertical heat transport by perturbation circulations cause maximum growth of perturbation kinetic energy to lead maximum loss of perturbation available potential energy by about 3 hours. The maximum vertical advective cooling, the horizontal-mean cloud-related heating, and perturbation radiative processes

cause maximum loss of perturbation moist available potential energy to lead maximum loss of the horizontal-mean moist available potential energy by about 1 hour. Consequently, the maximum gain of perturbation kinetic energy leads the maximum loss of horizontal-mean moist available potential energy by about 4–5 hours (about half of the lifetime of the simulated convection).

2.3. *Diurnal variation of tropical oceanic convection*

The diurnal variation of tropical oceanic convection is one of most important phenomena in tropical variability, and plays a crucial role in regulating tropical hydrological and energy cycles. The dominant diurnal signal is the nocturnal peak in precipitation that occurs in the early morning (see the review in Sui *et al.*, 1997a). Kraus (1963) emphasized the role of radiative forcing in the diurnal variation, and suggested that solar heating and IR cooling tend to suppress convection during daytime and enhance convection during nighttime respectively. Gray and Jacobson (1977) suggested that the diurnal variation of convection is a result of a synoptic-scale dynamic response to cloud radiative forcing (the radiational differences between cloudy regions and clear-sky regions). The cloud radiative forcing causes upward motion and convection during nighttime through the low-level convergence.

Sui *et al.* (1997a) conducted an analysis using the observational data from TOGA COARE. The data are first categorized into the disturbed and undisturbed periods by calculating the standard deviation of brightness temperature measured by the Geostationary Meteorological Satellite (GMS), operated by the Japanese Meteorological Agency. Over the disturbed periods, the total surface rain rate as well as convective and stratiform rain rates reach the maxima at 0300 local standard time (LST). Fractional cover for stratiform clouds has a maximum at 0300 LST whereas fractional cover for convective clouds does not show a significant diurnal variation. Diurnal variation of the rain rate histogram shows that the evolution of nocturnal rainfall has a growing phase from 2200 to 0300 LST, when a wide range of convection (the rain rate is larger than $0.5\,\mathrm{mm\,h^{-1}}$) becomes enhanced with most occurrences within 0.5–$5\,\mathrm{mm\,h^{-1}}$. The nocturnal rainfall is associated with anomalous ascending motion in the layer between 500 and 200 mb at 0400 LST. Over the undisturbed periods, the surface rain rate is very small, but shows a maximum from 1200 to 1800 LST. Diurnal variation of the rain rate histogram shows that the evolution of afternoon rainfall has a growing phase from 1200 to 1800 LST, while most occurrences of rain rates are within 0.5 to $5\,\mathrm{mm\,h^{-1}}$. The afternoon rainfall peak is associated with the maximum SST after the solar radiation flux reaches the maximum. A schematic summary of the nocturnal maximum convection in the disturbed period and afternoon clouds and showers in the undisturbed period is shown in Fig. 1. Based on the observational analysis, the nocturnal rainfall peak is suggested to be related to the destabilization by radiative cooling during nighttime and the falling temperature that makes more precipitable water available for the surface precipitation.

Xu and Randall (1995) performed a study using a cumulus ensemble model (CEM), and suggested that nocturnal convection results from a direct radiation–convection interaction in which solar absorption by clouds stabilizes the atmosphere (Randall *et al.*, 1991). Tao *et al.* (1996) performed a study of cloud–radiation mechanisms in the tropics and mid-latitudes using the Goddard cumulus ensemble (GCE) model. They emphasized the increase of surface precipitation by IR cooling as a result of increased relative humidity.

Sui *et al.* (1998a) conducted the cloud-resolving simulations to test their nocturnal rainfall mechanism. An experiment with the

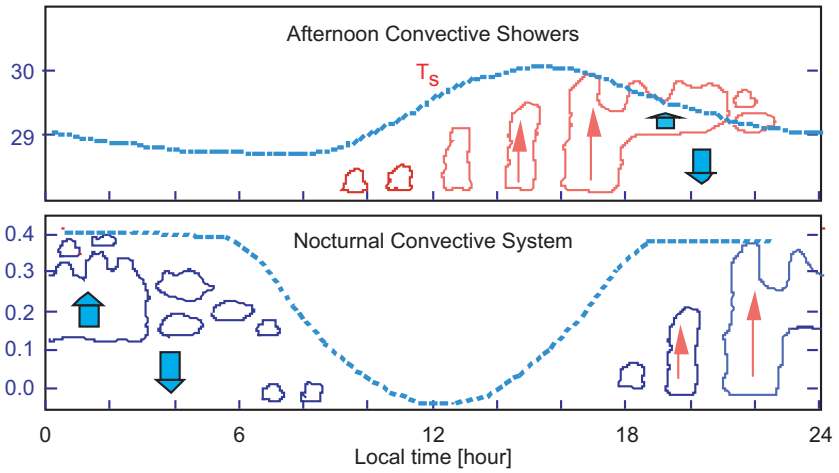

Figure 1. Schematic diagram of diurnal variations of convection during the disturbed (upper panel) and undisturbed (lower panel) periods. The dashed curve in the lower panel indicates the time rate of change of the saturation columnar water vapor amount, $-\partial W^*/\partial t$, corresponding to the diurnal cycle of temperature distribution. This quantity represents a direct effect of the radiative cooling/heating cycle on available precipitable water (APW), or a change of APW in the first step. The convective response to the direct forcing can induce further changes in temperature and moisture that lead to a corresponding change of APW in the second step. Since observed and simulated diurnal variations of convection are evidently in phase with the idealized cycle, the curve is regarded as a good theoretical limit for diurnal rainfall. The dashed curve in the lower panel indicates the diurnal cycle of sea surface temperature.

imposed large-scale ascending motion and a time-invariant SST generated a positive rainfall anomaly in the night and a negative rainfall anomaly in the day. The simulated maximum rain rate occurs around 0200 LST. Two additional experiments are carried out: one experiment with a zero imposed vertical velocity and a time-invariant SST, and the other with the cloud–radiation interaction suppressed. All three experiments show a dominant nocturnal rainfall maximum despite the experiments with very different external forcings and interaction processes. The results imply that cloud–radiation interaction does not play a crucial role in the formation of the nocturnal rainfall peak. The common feature in all of these experiments is the falling temperature induced by the nocturnal radiative cooling in the absence of the solar radiative heating. Thus, these numerical experiments support the suggestion of Sui *et al.* (1997a) that the nocturnal rainfall peak is related to more (less) available precipitable water in the night (day) as a result of the diurnal cooling/heating cycle (Fig. 1, lower panel). Sui *et al.* also conducted the experiment with zero imposed vertical velocity and a zonally uniform, diurnally varied SST and found that the simulated diurnal variations still have a nocturnal rainfall maximum but with a weaker magnitude and a secondary rainfall peak in the afternoon. This indicates that the maximum SST in the afternoon induces the unstable atmosphere that eventually leads to the rainfall peak (Fig. 1, upper panel).

2.4. *Cloud clustering and microphysical processes*

Lau *et al.* (1991) analyzed infrared radiance measurements at the cloud top from the Japanese GMS to study the structure and propagation of tropical cloud clusters over the equatorial western Pacific. The observed cloud clusters display a hierarchy of collective motions at time scales of 1 day, 2–3 days, and 10–15 days, respectively. The 1–15-day time scale is closely

related to the intraseasonal oscillation, and their super cloud clusters propagate eastward along the equator from the Indian Ocean to the western Pacific all around the global tropics. The cloud clusters embedded in the super cloud clusters have the 2–3-day time scale, and propagate in the opposite direction to the super cloud clusters. The diurnal time scale is most significant in the cloud clusters, in which the signals are more pronounced over the continent than over the open ocean.

Sui and Lau (1992) analyzed the First GARP Global Experiment IIIb circulation data along with the Japanese GMS-1 IR data to study the multiscale variability in the atmosphere over the tropical western Pacific during the 1979 Northern Hemisphere. Two intraseasonal oscillations propagate eastward from the Indian Ocean to the western Pacific. Over the western Pacific warm pool, the intraseasonal oscillations develop into quasi-stationary systems with the enhanced rotational circulations. The intraseasonal oscillations interact with regional and synoptic-scale systems such as monsoon circulations. The intraseasonal oscillations also excite the 2–4-day disturbances. Sui and Lau also found that the diurnal signal becomes strong when the intraseasonal oscillation loses the intensity whereas the opposite is true.

To investigate the relevant cloud clustering processes (formation and evolution of cloud ensembles), Peng *et al.* (2001) performed a numerical experiment using a two-dimensional cloud ensemble model covering a basin-scale domain (15 360 km) with prescribed warm SST surrounded by cold SST, to mimic the equatorial western Pacific. The model used an open lateral boundary. Under the condition of no prescribed basic zonal flow and no initial perturbation, deep convective clouds develop in hierarchical clustered patterns, which are limited to the area of warm SST above 28°C. The most fundamental cloud cluster in the model has a horizontal scale of a few hundred kilometers, in which new cumulus clouds are generated at the leading edge of a propagating surface cold pool, the "gust front." It may last for days and propagate for a long distance if the background flow is broad and persistent, as is the case in the low-level convergence zone of the SST-induced background flow.

The largest hierarchical propagating cloud systems in the model have horizontal scales of up to 3000 km and consist of up to four cloud clusters that are generally of the gust-front type. The constituent cloud clusters are generated intermittently and have life spans of 12–36 h. The internal heating of the constituent clusters collectively induces an overall troposphere-deep gravity wave (Mapes and Houze, 1993; Mapes, 1993). The overall wave travels in the direction of the tropospheric deep shear at a speed determined by the thermodynamic asymmetry in the wave created by the transition from warm and moist incoming air in the front to drier and cooler air in the rear.

The development of new cumulus clusters in the gust-front region of the hierarchical system is due to the combined effect of the overall wave and the gravity waves excited by the constituent clusters on the lower-tropospheric stability. When there are no interruptions from outside the cloud system, new cloud clusters develop intermittently from shallow disturbances hundreds of kilometers ahead of the existing deep convection. The resulting hierarchical cloud pattern resembles the observed equatorial super cloud cluster (SCC) in the time–longitude diagram. However, the life spans of the constituent clusters of the simulated system are shorter than that in the observed SCC.

The dynamic processes for cloud clustering are intimately coupled to microphysical processes. This coupling may be revealed by water- and ice-cloud contents and their corresponding microphysics. This is investigated in several companion papers. Li *et al.* (2002c) simulated the cloud clusters using the two-dimensional cloud-resolving model with the imposed forcing from the TOGA COARE data

during the disturbed period. The cloud clusters move westward, while the embedded individual clouds propagate eastward. Along with the westward propagation and during the development of tropical convection, the area-mean vertical velocity profiles exhibit the major ascending motion below 500 mb in the western half of the cloud, and the maximum ascending motion between 300 and 500 mb in the eastern half, indicating that the western half of the cloud undergoes the deep convective development whereas the anvil cloud grows in the eastern half. The surface rainfall is much larger in the western half than in the eastern half. The amount of water hydrometeors is much larger than that of ice hydrometeors in the western half, whereas ice and water hydrometeors have similar amounts in the eastern half. The analysis of the rainwater budget reveals that the collection of cloud water by raindrops is a major process for the surface rainfall, and thus the water hydrometeor processes are dominant in the deep convective clouds in the western half, whereas both the collection of cloud water by raindrops and the melting of precipitation ice into raindrops are responsible for the surface rainfall in the anvil clouds in the eastern half.

The simulations show that the performance of cloud-microphysical parametrization schemes has the direct, crucial impacts on the simulations of cloud clusters in the genesis, evolution, propagation, and amplitudes. However, the computation of the full set of cloud-microphysical equations is time-consuming. Li *et al.* (2002c) found from their analysis of cloud-microphysical budgets that in the deep tropical convective regime, the magnitudes of 12 terms out of the total of 29 cloud-microphysical processes are negligibly small. Thus, they proposed a simplified set of cloud-microphysical equations, which saves 30–40% of CPU time. The neglected terms in the simplified set include the accretion of cloud ice and snow by raindrops, the evaporation of melting snow, the accretion of cloud water and raindrops by snow, the accretion of raindrops and the homogeneous freezing of cloud water by cloud ice, the accretion and freezing of raindrops by graupel, the growth of cloud water by the melting of cloud ice, and the growth of cloud ice and snow by the deposition of cloud water. An experiment with the simplified set of cloud-microphysical equations was conducted and compared to an experiment with the original set of cloud-microphysical equations. The two experiments show similar time evolution and magnitudes of temperature and moisture profiles, surface rain rates including stratiform percentage and fractional coverage of convective, raining and nonraining stratiform clouds. This suggests that the original set of cloud-microphysical equations could be replaced by the simplified set in simulations of tropical oceanic convection.

Sui and Li (2005) analyzed the same TOGA COARE experiment performed by Li *et al.* (2002c) to show that interaction between ice and water clouds is crucial in determining the life span of deep convective and stratiform clouds and the evolution of cloud clusters. They defined a cloud ratio that is the ratio of the vertically integrated content of ice clouds (ice water path, IWP) to the liquid water path (LWP) to study the ice–water-hydrometeor interaction processes and their impacts in the development of convective and stratiform clouds. Clouds become more stratiform when the tendency of the cloud ratio is positive whereas they become more convective when the tendency of the cloud ratio is negative. The advantage of the definition of the cloud ratio is to mathematically derive a tendency equation of the cloud ratio based on the prognostic cloud equations in the cloud-resolving framework. The derived cloud ratio budget indicates that the tendency of the cloud ratio is determined by the vapor condensation and deposition (cloud sources), rainfall and evaporation (cloud sinks), and conversion between ice and water hydrometeors including melting of precipitation ice to raindrops and accretion of cloud water by precipitation ice. The analysis reveals that the

tendency of the cloud ratio is mainly determined by the vapor condensation and deposition during the genesis and decay of the tropical convection when the system is relatively weak, whereas the tendency is controlled by the convection process during the development of tropical convection, when the system is relatively strong.

Sui *et al.* (2007a) proposed using threshold values of the cloud ratio to separate the convective component of the precipitation from the remainder. The cloud variables (IWP, LWP, and their ratio) are physically linked to the cloud microphysics, as demonstrated by an analysis of simulated cloud microphysics budgets in the same two-dimensional cloud-resolving model experiment subject to the imposed forcing from the TOGA COARE. Their analysis suggests that rainfall can be designated convective when the corresponding value of the cloud ratio is smaller than 0.2, or the value of IWP is larger than 2.55 mm. The remaining grids are classified as mixed and stratiform when the corresponding range of the cloud ratio is 0.2–1.0, and greater than 1, respectively. The new partition method is evaluated by the vertical velocity (w) data. The frequency distribution of w shows that w in the convective region has a wide distribution, with maximum values exceeding $15\,\mathrm{m\,s^{-1}}$. In the designated stratiform region, the distribution is narrow, with absolute values of w confined within $5\,\mathrm{m\,s^{-1}}$. The statistics of w and the budgets of cloud microphysics are consistent with corresponding physical characteristics of the convective and stratiform regions of precipitation. The w distribution in the mixed region exhibits features more convective than stratiform, indicating a transition stage of convective development. But the consideration of features like fractional cloud covers, rain rates, vertical velocity profiles, and the corresponding wave response leads us to regard the mixed and stratiform regions as the nonconvective region.

2.5. *Precipitation efficiency*

Precipitation efficiency is an important physical parameter for measuring the interaction between convection and its environment (Doswell *et al.*, 1996; Ferrier *et al.*, 1996; Tao *et al.*, 2004). Its definition may vary. For large-scale applications involving cumulus parametrization (e.g. Kuo, 1965, 1974), the precipitation efficiency is defined as the ratio of the surface rain rate to the sum of the surface evaporation and vertically integrated moisture convergence, and is referred to as large-scale precipitation efficiency (LSPE). LSPE is similar to the precipitation efficiency defined by Braham (1952). For cloud-resolving models with cloud-microphysical parametrization schemes (e.g. Li *et al.*, 1999), the precipitation efficiency can be defined as the ratio of the surface rain rate to the sum of the vertically integrated condensation and deposition rates. This is referred to as cloud microphysics precipitation efficiency (CMPE). CMPE is similar to the precipitation efficiency defined by Weisman and Klemp (1982) and Lipps and Hemler (1986).

Li *et al.* (2002a) analyzed the domain-mean CMPE and found that the LSPE could be more than 100%, whereas the CMPE is less than 100%. The statistical analysis shows that the ratio of the CMPE to the LSPE is 1.2. The precipitation efficiency may depend on the environmental conditions and the strength of convection. Ferrier *et al.* (1996) showed that wind shear and updraft structure play an important role in determining the precipitation efficiency. Li *et al.* (2002a) showed that the CMPE increases with increasing mass-weighted mean temperature and surface rain rate. This suggests that precipitation processes are more efficient for the heavy rain regime in a warm environment.

Since the LSPE and the CMPE are expected to be the same based on physical considerations, the difference in Li *et al.* (2002a) is attributed in Sui *et al.* (2005) to the horizontal hydrometeor

advection that is excluded in the domain-mean CMPE due to the cyclic lateral boundary condition. Sui *et al.* (2005) analyzed the grid data from the two-dimensional cloud-resolving simulations with the imposed TOGA COARE forcing and the three-dimensional MM5 cloud-resolving simulation of Typhoon Nari (Yang and Huang, 2004). The analysis of two-dimensional grid data through the root-mean-square differences and linear correlation coefficients shows that the sum of vapor condensation and deposition rates is approximately balanced by the sum of surface evaporation and vertically integrated moisture convergence. This relation leads to the statistical equivalence between the CMPE and the LSPE.

Analysis of the two-dimensional simulation further shows that the additional hydrometeor converging into the atmospheric column would make the precipitation efficiency larger. When the hydrometeor convergence becomes the dominant term in the cloud budget, the CMPE can be larger than 100%, as found in light-rain conditions ($<5\,\mathrm{mm\,h^{-1}}$). On the other hand, a loss of clouds due to hydrometeors diverging out to the neighboring columns would make the CMPE smaller. This occurs mostly in heavy-rain conditions ($>5\,\mathrm{mm\,h^{-1}}$). The three-dimensional simulation of Typhoon Nari (2001) with more intense precipitation (compared to the TOGA COARE tropical convection) generally supports the two-dimension results.

Sui *et al.* (2007b) revisited the issue using the same two-dimensional cloud-resolving model simulation. They proposed more complete definitions of precipitation efficiency based on either the moisture budget (LSPE2) or the hydrometeor budget (CMPE2), which include all sources related to surface rainfall processes. They reached the following conclusions: (1) LSPE2 and CMPE2 range from 0 to 100%; (2) LSPE2 and CMPE2 are highly correlated; (3) LSPE2 and CMPE2 are insensitive to the spatial scales of averaged data, and moderately sensitive to the time period of averaged data; (4) the simplified precipitation efficiencies of LSPE1 and CMPE1 appear to be good enough measures of precipitation efficiency in the heavy-rain conditions. CMPE2 (or CMPE1) is a physically more straightforward definition of precipitation efficiency than LSPE2 (or LSPE1). But the former can only be estimated in models with explicit parametrization of cloud microphysics which is model dependent, while the latter may be estimated based on currently available assimilation data of satellite and sounding measurements.

3. Air–Sea Exchange and Ocean Mixing at the Diurnal and Intraseasonal Scales

Lau and Sui (1997) and Sui *et al.* (1997b) analyzed the COARE data and found that the dry and wet phases in the atmospheric precipitable water are associated with the passage of the intraseasonal oscillations during the TOGA COARE. The passage of the intrareasonal oscillations also affects the surface radiative and heat fluxes that impact the ocean mixing processes and thus the upper-ocean stratification. The 2–3-day disturbances and diurnal cycles are phenomena with the dominant time scales during the wet phase, whereas the diurnal cycles in the SST are regularly forced by the diurnal solar radiative flux in the day and outgoing radiative and heat fluxes in the night during the dry phase (Fig. 2). This implies that the vertical solar absorption profile in the upper ocean plays an important role in determining the mixed-layer depth and the amount of solar absorption in the mixed layer, which eventually control the evolution of ocean mixed-layer temperature.

Sui *et al.* (1997b) employed a mixed-layer model to study the role of the vertical solar absorption profile in the diurnal ocean temperature simulations and their impacts on the intraseasonal variability. Owing to the asymmetric diurnal variation for shoaling and deepening

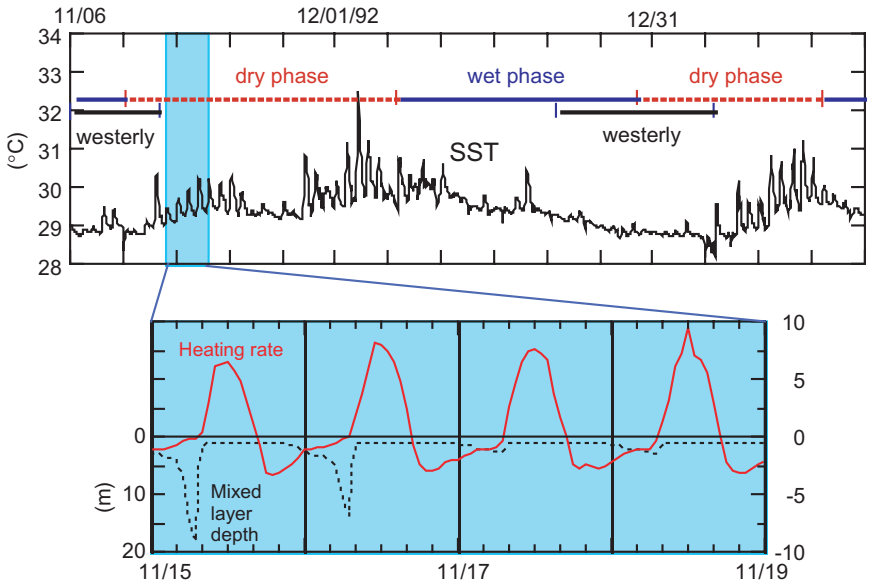

Figure 2. Time series of observed SST during the TOGA COARE (upper panel) and the simulated heating rate (solid) and mixed-layer depth (dashed) during selected COARE periods (lower panel).

of the mixed layer, the cumulative effect of diurnal mixing cycles is essential to maintaining a stable upper-ocean thermal stratification and to simulating a realistic evolution of mixed-layer and temperature at the intraseasonal time scale. Further sensitivity tests of mixed layer to diurnal cycles indicate that the inclusion of diurnal convective–radiative processes in the atmosphere–ocean system in the coupled models affects the capability of simulating intraseasonal variability.

The salinity contributes more to the density stratification than does the temperature, which is responsible for upper-ocean stability. Li *et al.* (1998) further included the salinity in the ocean mixed-layer modeling to examine the impacts of the precipitation and associated upper-ocean salinity stratification on the ocean mixed layer. The inclusion of salinity and precipitation-induced fresh water flux in the simulation shows that much deeper mixing occurs when rainfall appears during the night since the fresh water flux induces a much shallower mixed layer with a large deepening rate, which is consistent with the observations. The inclusion of the salinity stratification could cause warmer water entrained into the ocean mixed layer since the salinity stratification maintains the upper-ocean stability, whereas the exclusion of salinity in the simulation only shows entrainment of cold water into the ocean mixed layer since the thermal stratification accounts for the upper-ocean stability. Because the Kraus–Tuner mixing parametrization scheme (Niiler and Kraus, 1977) requires both thermal and saline stratifications to determine the mixed-layer depth, Li *et al.* carried out decoupled salinity experiments to examine the effect of thermal stratification on the saline structure. The experiments reveal that when the fresh water input is large, the salinity variations simulated with and without the thermal stratification can be significantly different. The difference in the salinity could be 0.2 PSU. The simulations indicate that the inclusion of precipitation-induced fresh water flux and salinity stratification improves the simulation of thermal evolution in the ocean mixed layer.

Sui *et al.* (1998b) used a mixed-layer model along with the estimate of surface forcing obtained from the TOGA COARE to estimate the amount of heat absorbed in the observed mixed layer to maintain the observed amplitudes of SST which is largely dependent on the depth-dependent solar heating. The simulated amplitude of the diurnal cycle of mixed-layer temperature ($< 1°C$) is significantly smaller than the observed amplitude (1–3°C), implying that the mixed layer in the simulation does not absorb enough solar heat. They found that more than 39% of the net surface solar irradiance is absorbed within the first 0.45 meters in order to maintain the observed SST, which is higher than previous estimates. The vertical profile of solar absorption is then modified, and the simulation with the modified solar profile yields more realistic amplitudes of the SST at both the diurnal and intraseasonal time scales.

4. Coupled Boundary Layer and Forced Oceanic Responses

Sui *et al.* (1991) developed an equilibrium model to study the coupled ocean–atmosphere boundary layer in the tropics, which consists of a one-dimensional thermodynamic atmospheric model for a partially mixed, partially cloudy convective boundary layer (CBL), Betts and Ridgway, 1988; 1989 and an oceanic mixed-layer (OML) model. Two experiments were performed with sea surface temperature (SST) specified. They solve the equilibrium state of the coupled system as a function of SST for a given surface wind, and as a function of surface wind for a given SST. The increases in SST lead to the increase in the depth of the convective boundary layer owing to the increase in the water vapor. The moistened and deepened CBL leads to a reduced net surface heat flux which is balanced by weakened upwelling and causes a deepened ocean mixed layer. The increase in surface wind also causes the increase in the depth of the ocean mixed layer and the decrease in the upwelling below the ocean mixed layer. But this is due to the generation of turbulence kinetic energy and the decrease in the net downward heat flux. The latter is due to the nonlinear change of air–sea humidity difference with increasing surface wind, such that a deepening CBL reduces the downward solar radiation and increases the downward longwave radiation at the surface. In another two experiments, the coupled model was solved iteratively as a function of surface wind for a fixed upwelling, and for a fixed mixed-layer depth (h). SST falls with increasing wind in both experiments, but the fall is gradual in the fixed upwelling condition because the depth is allowed to deepen and the cooling is spread over a larger mass of water, while the fall is steeper in the other experiment because h is fixed. The decrease of evaporation with increasing wind in fixed h condition leads to a very dry and shallow CBL. More experiments with surface wind and SST (upwelling) prescribed as a function of longitude similar to the observed values across the Pacific give realistic gradients of mixed-layer depth and upwelling (SST). The work quantifies the sensitivity of the equilibrium state of the coupled system to the coupling of the boundary layers, and provides a framework for understanding physical processes in the CBL and OML in coupled models.

Li *et al.* (2000) developed a coupled ocean–cloud-resolving atmosphere model to study effects of precipitation on ocean mixed-layer temperature and salinity. When the effects of fresh water flux and salinity were included in the coupled model, differences in the horizontal-mean mixed-layer temperature and salinity between 1D and 2D experiments were about 0.4°C and 0.3 PSU, respectively. The mean salinity difference was larger than the mean temperature difference in terms of their contributions to the mean density difference. In the 2D experiment, the surface heat flux showed a significant diurnal signal with the dominance of downward solar radiation during daytime and upward flux (longwave, sensible and latent heat

fluxes) during nighttime at each grid, although the amplitude was affected by precipitation. Thus, there was a strong thermal correlation between grids. Narrow cloudy areas were surrounded by broad, cloud-free areas. Horizontal-mean precipitation could occur, whereas the precipitation may not occur in most of the integration period. Thus, there is a very low correlation between horizontal-mean and grid values of the fresh water fluxes. Since the rain rates have significant spatial variations, the fresh water flux has much larger spatial fluctuations than the saline entrainment. Therefore, the fresh water flux determines large spatial salinity fluctuations, which contributes to a large mean salinity difference between the 1D ocean model experiment and the 2D ocean model experiment.

Sui *et al.* (2003) investigated the impacts of high-frequency surface forcing on the upper ocean over the equatorial Pacific by conducting a nonlinear reduced-gravity isopycnal ocean circulation simulations with the daily and monthly mean forcings, respectively, and found that the daily-forcing experiment produces a colder SST than does the monthly-forcing experiment, and the difference in the SST between the two experiments is generated in the first year integration. The negative difference in the SST between the daily-forcing and monthly-forcing experiments in the western Pacific is primarily caused by enhanced latent heat loss due to the transient winds. Over the eastern Pacific, the zonal thermal advection accounts for the difference, while other terms are large but cancel each other out. Relative to the monthly forcing, the effect of daily forcing is found to (1) enhance vertical mixing and reduce vertical shear in the upper ocean; (2) reduce net heat into the ocean through two contrasting processes — increased surface latent heat loss induced by transient winds, and a colder SST (due to stronger mixing) reducing surface heat loss; (3) weaken meridional thermal advection through more active instability waves; (4) change mixed-layer depth so that the temperature in the simulation with the daily forcing is warmer around the thermocline.

5. Representation of Convective–Radiative Processes in Climate Models

The research results discussed in this review represent a one-way interaction approach for process models to study the physical processes interacting with climate oscillations. The acquired knowledge forms a basis for improving the representation of these physical processes in climate models, and also motivates the next-step approach to examining the radiative–convective (two-way) interaction with climate dynamics in large-scale models. Indeed, since the original attempt by Sundqvist (1978) to include prognostic cloud water content for parametrizing nonconvective condensation, there has been increasing research attempts to incorporate detailed microphysical processes in weather and climate models. The trend is to treat cloud water and/or ice content as a prognostic variable which is governed by microphysical processes (e.g. Tiedtke, 1993; Del Genio *et al.*, 1996; Fowler *et al.*, 1996; Sud and Walker, 1999, 2003; Zhao and Carr, 1997). This approach allows the storage and full life cycle of cloud water, and a better cloud–radiation linkage through interactive cloud optical properties. While this approach provides a more physically based framework for representing the physical processes, it also introduces a number of microphysical parameters absent from the simpler approaches. Thus, a great deal of effort is required to implement a prognostic cloud parametrization scheme in climate models, and to validate the scheme against various observational data sets.

Another approach to incorporating detailed convective processes in weather and climate models is through directly resolving convective dynamics in the GCM, such as "super-parametrization" (Grabowski and Smolarkiewicz, 1999; Grabowski, 2001;

Khairoutdinov and Randall, 2001). This approach is to implement a cloud-resolving model (CRM) inside each grid box of a global model. The CRM (so far two-dimensional) does not fill the global model's grid box. Instead, it occupies only part of the grid box. The advection terms computed at each grid of the global model is imposed in the CRM as heat and moisture source/sink. In return, the CRM computes cloud ensemble statistics. In this way, the super-parametrization provides a framework for coupling convective–radiative processes with large-scale dynamics all at the physical time and space scales of the convective process. But this approach also introduces many problems different from those of simpler cumulus parametrization. See Randall *et al.* (2003) for details.

At the GSFC, continual efforts have been made to improve the representation of convective–radiative processes on a multi–model framework. One approach is to run the finite-volume general circulation model (fvGCM; Lin, 2004) at 1/8 of a degree (about 12 km) to resolve convective vortices in the global model context. The model is capable of simulating realistic tropical cyclones in the weather prediction model (Altas *et al.*, 2005). An attempt at super-parametrization in the fvGCM is also being examined.

Another important effort at the GSFC is to utilize satellite measurements to advance cloud-climate feedback study in climate models. Lau and Wu (2003) performed an analysis of satellite data from the Tropical Rainfall Measuring Mission (TRMM; Simpson *et al.*, 1988). They found that warm rain accounts for 31% of the total rain amount and 72% of the total rain area in the tropics, and that there is a substantial increase in the precipitation efficiency of light warm rain as the sea surface temperature increases, but the precipitation efficiency of heavy rain associated with deep convection is independent of the sea surface temperature. This implies that in a warmer climate, there may be more warm rain, at the expense of less cloud water available for middle and high level clouds. The study points out a possible need to pay attention to resolving the melting/freezing zone in convection to simulate and better understand the role of cumulus congestus in tropical convection, and its sensitivity to SST, and global warming. Lau *et al.* (2005) performed a sensitivity test of GCM dynamics to the microphysics parameter of autoconversion. The result shows that a faster autoconversion rate leads to enhanced deep convection, more warm rain but less cloud over oceanic regions, and an increased convective-to-stratiform rain ratio over the entire tropics. The resultant vertical differential heating destabilizes the tropical atmosphere, producing a positive feedback, resulting in more rain and an enhanced atmospheric water cycle over the tropics. The feedback is maintained via secondary circulations between convective tower and anvil regions (cold rain), and adjacent middle-to-low cloud (warm rain) regions. The lower cell is capped by horizontal divergence and maximum cloud detrainment near the freezing/melting (0°C) level, with rising motion (relative to the vertical mean) in the warm rain region connected to sinking motion in the cold rain region. The upper cell is found above the 0°C level, with induced subsidence in the warm rain and dry regions, coupled to forced ascent in the deep convection region. The above result reveals that warm rain plays an important role in regulating the time scales of convective cycles, and in altering the tropical large-scale circulation through radiative dynamic interactions. Reduced cloud–radiation feedback by a faster autoconversion rate results in intermittent but more energetic eastward-propagating Madden and Julian oscillations (MJO's). Conversely, a slower autconversion rate, with increased cloud radiation produces MJO's with more realistic westward-propagating transients embedded in eastward-propagating supercloud clusters.

Super-parametrization is an intermediate approach to representing convective–radiative

processes in a global model, between a prognostic cloud scheme and a global cloud-resolving model. If computational resources allow, it is most straightforward to develop an ultrahigh-resolution nonhydrostatic climate model that can resolve clouds with explicit microphysics. Global nonhydrostatic models are being developed at many institutions. In particular, a global nonhydrostatic grid model with icosahedral structure is being developed in Japan (Satoh *et al.*, 2005). This model is intended for high-resolution climate simulation, so the numerical scheme is designed for conserving mass and energy. Global simulations with cloud-resolving physical processes (cloud microphysics, radiation, and boundary layer processes) have been performed on an aqua planet setup with grid intervals of 7 km and 3.5 km. The model simulates reasonable features in the tropics, like the diurnal cycle of precipitation, hierarchical structure of clouds, and intraseasonal oscillations (Tomita *et al.*, 2005). The model's response to SST warming has also been investigated by Miura *et al.* (2005).

6. Relevance to Climate Variability and Future Perspectives

In this article, the authors' research results in the past 15 years in the tropics are highlighted. Reviewed are convective–radiative processes including climate equilibrium study, tropical convective responses to radiative and microphysical processes, the diurnal cycle, cloud clustering and associated cloud-microphysical processes, precipitation efficiency, air–sea exchanges and ocean mixing processes at diurnal-to-intraseasonal scales, and coupled boundary layer and forced oceanic responses. These physical processes coupled with the tropical wave dynamics have been recognized as key mechanisms in maintaining climate variability in the tropical ocean atmosphere, as exemplified in the following scientific issues.

One of the important issues is the response of water vapor and clouds to anthropogenic changes of greenhouse gases and aerosols. While many observational analyses and GCM simulations support a positive water vapor feedback on a global scale (e.g. Zhang *et al.*, 1996; Soden, 1997; Inamdar and Ramanathan, 1998), some studies suggest that this water vapor feedback may be overestimated or even negative (Lindzen, 1990; Lindzen *et al.*, 2001). Being inseparable from water vapor feedback, cloud-radiative forcing is another important climate feedback process. However, the effect of cloud feedback on climate change is equally if not more controversial than water vapor feedback. Studies of cirrus (or high) clouds and associated radiative effect on tropical climate do not even agree on the sign of the cloud feedbacks (e.g. Prabhakara *et al.*, 1993; Ramanathan and Collins, 1991; Kiehl, 1994). A synthesis of the above studies reveals that water vapor and cloud feedbacks depend on the relative areas of cloudy/moist regions versus clear/dry regions, as well as on cloud properties (type, height, optical thickness) and water vapor distribution within the clear and cloudy regimes.

Another issue is the impact on the simulations of global mean climate and climate variability through the improved representation of cloud-related processes in GCM's using the CRM simulations. Wu and Moncrieff (2001) used the CRM to identify the biases in the radiation and cloud scheme used in the GCM. Liang and Wu (2005) used the CRM to evaluate the treatment of subgrid cloud distribution in the radiation scheme; Wu and Liang (2005) used the CRM results to improve the climate simulations with the inclusion of effects of subgrid cloud–radiation interaction. With the inclusion of the convective momentum transport (CMT) scheme derived from the CRM simulations, the tropical convection and the Hadley circulation are better-represented in GCM's (Zhang and Wu, 2003; Wu *et al.*, 2003).

The other issue is the multiscale air–sea interaction processes associated with the

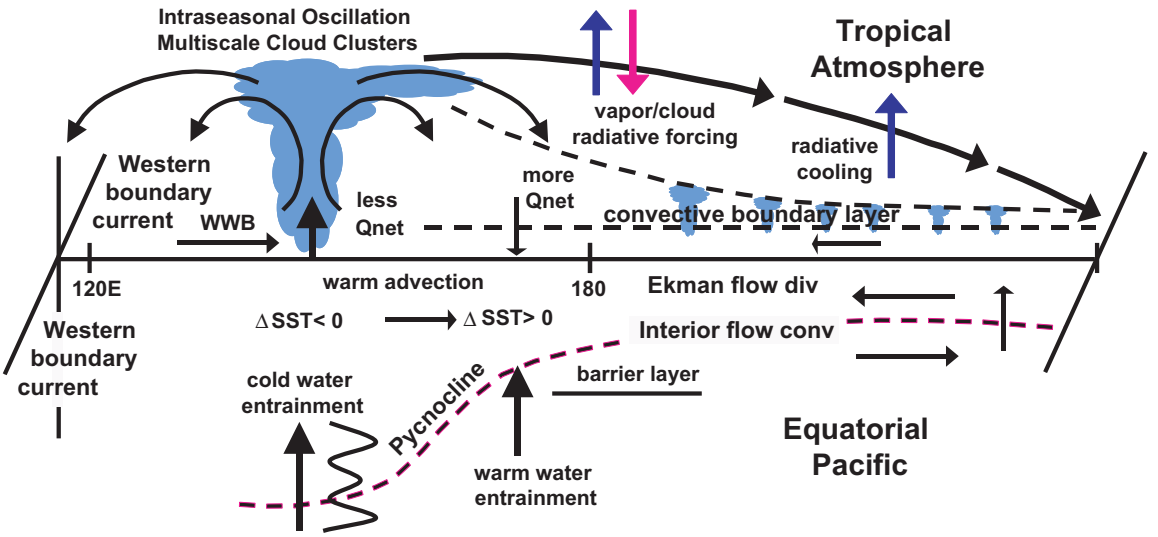

Figure 3. Summary diagram for the convective–radiative-mixing processes in the tropical ocean–atmosphere.

intraseasonal oscillations in the warm pool region illustrated in Fig. 3. Because the precipitation rate is greater than the evaporation rate over the equatorial western Pacific warm pool, whereas it is smaller over the eastern Pacific, a barrier layer appears year round within the warm pool (e.g. Lukas and Linstrom, 1991; Ando and McPhaden, 1997; Vialard and Delecluse, 1998ab). The barrier layer insulates the penetrated solar energy in the barrier layer from the mixed layer. As an intraseasonal oscillation propagates eastward to the warm pool, the strong westerly wind burst causes strong vertical mixing in the upper ocean that destroys the barrier layer and entrains cold water beneath into the mixed layer. The rapid decay of the intraseasonal oscillation near the dateline means that there is no impact on the barrier layer there and vertical entrainment would entrain the warm water beneath into the mixed layer. These entrainment processes together with the surface air–sea interaction processes illustrated in Fig. 3 may result in a cool SST anomaly over the warm pool and a warm SST anomaly near the dateline. The SST anomalies in turn induce an eastward extension of atmospheric intraseasonal oscillations, and reduce easterly trade winds by weakening the overall zonal SST gradient. The air–sea interaction might strengthen and prolong the intraseasonal oscillation and play an important role in the development stage of ENSO, which could be phase-locked to the annual cycle.

The above discussion proposes some key climate processes to be addressed by more advanced models with more physical representations of convective, radiative, and mixing processes. In addition, it is important to utilize new observations like satellite measurements to advance cloud-climate feedback study in climate models (e.g. Lau *et al.*, 2005). There are also some critical issues related to convective–radiative-microphysical processes not discussed in this review article, and they deserve further investigation. For example, turbulence mixing in the boundary layer is still crudely parametrized in CRMs and needs to be improved. There are different time scales in the cloud-microphysical processes (condensation versus coalescence) and the probabilistic nature of microphysical processes that should be included in the microphysics parametrization (e.g. Chen and Liu, 2004). The cloud–aerosol interaction, which is not considered in most CRM's, needs to be studied comprehensively in the future.

Acknowledgements

We thank the two anonymous reviewers for their constructive comments, and are grateful for the continuous support of our research from the National Research Council in Taiwan, the National Aeronautics and Space Administration, the National Science Foundation, and the National Ocean and Atmosphere Administration in the US in the past 15 years. The GCE modeling work is mainly supported by the NASA Headquarters Physical Climate Program and the NASA TRMM. In particular, Dr. R. Kakar at NASA headquarters has continuously supported the model improvements and applications.

[Received 24 April 2006; Revised 16 May 2007; Accepted 27 July 2007.]

References

Ando, K., and M. J. McPhaden, 1997: Variability of surface layer hydrography in the tropical Pacific Ocean. *J. Geophys. Res.*, **102**, 23063–23078.

Arakawa, A., and W. H. Schubert, 1974: Interaction of a cumulus cloud ensemble with the large-scale environment. Part I. *J. Atmos. Sci.*, **31**, 674–701.

Atlas, R., O. Reale, B.-W. Shen, S.-J. Lin, J.-D. Chern, W. Putman, T. Lee, K.-S. Yeh, M. Bosilovich, and J. Radakovich, 2005: Hurricane forecasting with the high-resolution NASA finite volume general circulation model. *Geophys. Res. Lett.*, **32**, L03807, doi:10.1029/ 2004GL021513.

Betts, A. K., and M. J. Miller, 1986: A new convective adjustment scheme. Part II: Single column tests using GATE wave, BOMEX, ATEX and arctic airmass data sets. *Quart. J. Roy. Meteor. Soc.*, **112**, 692–709.

Betts, A. K., and W. Ridgway, 1988: Coupling of the radiative, convective and surface fluxes over the equatorial Pacific. *J. Atmos. Sci.*, **45**, 522–536.

Betts, A. K., and W. Ridgway, 1989: Climatic equilibrium of the atmospheric convective boundary layer over a tropical ocean. *J. Atmos. Sci.*, **46**, 2621–2641.

Braham, R. R., Jr., 1952: The water and energy budgets of the thunderstorm and their relation to thunderstorm development. *J. Meteor.*, **9**, 227–242.

Chen, J.-P., and S.-T. Liu, 2004: Physically based two-moment bulkwater parametrization for warm-cloud microphysics. *Quart. J. Roy. Meteor. Soc.*, **130**, 51–78.

Cheng, M.-D., and M. Yanai, 1989: Effects of downdrafts and mesoscale convective organization on the heat and moisture budgets of tropical cloud cluster. Part III: Effects of mesoscale convective organization. *J. Atmos. Sci.*, **56**, 3028–3042.

Chou, M.-D., D. P. Kratz, and W. Ridgway, 1991: IR radiation parametrization in numerical climate studies. *J. Climate*, **4**, 424–437.

Chou, M.-D., and M. J. Suarez, 1994: An efficient thermal infrared radiation parametrization for use in General Circulation Model. *NASA Technical Memorandum 104606*, Vol. 3, 85 pp.

Chou, M.-D., M. J. Suarez, C.-H. Ho, M. M.-H. Yan, and K.-T. Lee, 1997: Parameterizations for cloud overlapping and shortwave single-scattering properties for use in General Circulation and Cloud Ensemble Models. *J. Climate*, **11**, 202–214.

Del Genio, A. D., N.-S. Yao, W. Kovari, and K.-W. Lo, 1996: A prognostic cloud water parametrization for general circulation models. *J. Climate*, **9**, 270–304.

Doswell, C. A., III, H. E. Brooks, and R. A. Maddox, 1996: Flash flood forecasting: an ingredients-based methodology. *Wea. Forecasting*, **11**, 560–581.

Ferrier, B. S., J. Simpson, and W.-K. Tao, 1996: Factors responsible for different precipitation efficiencies between midlatitude and tropical squall simulations. *Mon. Wea. Rev.*, **124**, 2100–2125.

Fowler, L. D., D. A. Randall, and S. A. Rutledge, 1996: Liquid and ice cloud microphysics in the CSU general circulation model. Part I: Model description and simulated microphysical processes. *J. Climate*, **9**, 489–529.

Fu, R., A. D. Del Genio, W. B. Rossow, and W. T. Liu, 1992: Cirrus cloud thermostat for tropical sea surface temperatures tested using satellite data. *Nature*, **358**, 394–397.

Grabowski, W. W., X. Wu, and M. W. Moncrieff, 1996: Cloud-resolving model of tropical cloud systems during Phase III of GATE. Part I: Two-dimensional experiments. *J. Atmos. Sci.*, **53**, 3684–3709.

Grabowski, W. W., 2001: Coupling cloud processes with convection parameterizaiton (CRCP). *J. Atmos. Sci.*, **58**, 978–997.

Grabowski, W. W., and P. K. Smolarkiewicz, 1999: CRCP: A cloud-resolving convection parametrization for modeling the tropical convective atmosphere. *Physica D*, **133**, 171–178.

Gray, W. M., and R. W. Jacobson, 1977: Diurnal variation of deep cumulus convection. *Mon. Wea. Rev.*, **105**, 1171–1188.

Hartmann, D. L., and M. L. Michelsen, 1993: Large-scale effects on the regulation of tropical sea surface temperature. *J. Climate*, **6**, 2049–2062.

Hsie, E. Y., R. D. Farley, and H. D. Orville, 1980: Numerical simulation of ice phase convective cloud seeding. *J. Appl. Meteor.*, **19**, 950–977.

Inamdar, A. K., and V. Ramanathan, 1994: Physics of greenhouse effect and convection in warm oceans. *J. Climate*, **7**, 715–731.

Johnson, D., W.-K. Tao, J. Simpson, and C.-H. Sui, 2002: A study of the response of deep tropical clouds to mesoscale processes: Part I: Modeling strategies and simulations of TOGA-COARE convective systems. *J. Atmos. Sci.*, **59**, 3492–3518.

Khairoutdinov, M. F., and D. A. Randall, 2001: A cloud-resolving model as a cloud parametrization in the NCAR Community Climate System Model: Preliminary results. *Geophys. Res. Lett.*, **28**, 3617–3620.

Kiehl, J. T., 1994: On the observed near cancellation between longwave and shortwave cloud forcing in tropical regions. *J. Climate*, **7**, 559–565.

Klemp, J. B., and R. B. Wilhelmson, 1978: The simulation of three-dimensional convective storm dynamics. *J. Atmos. Sci.*, **35**, 1070–1093.

Koenig, L. R., 1971: Numerical modeling of ice deposition. *J. Atmos. Sci.*, **28**, 226–237.

Kraus, E. B., 1963: The diurnal precipitation change over the sea. *J. Atmos. Sci.*, **20**, 546–551.

Krueger, S. K., Q. Fu, K. N. Liou, and H.-N. S. Chin, 1995: Improvement of an ice-phase microphysics parametrization for use in numerical simulations of tropical convection. *J. Appl. Meteor.*, **34**, 281–287.

Kuo, H. L., 1965: On formation and intensification of tropical cyclones through latent heat release by cumulus convection. *J. Atmos. Sci.*, **22**, 40–63.

Kuo, H. L., 1974: Further studies of the parametrization of the influence of cumulus convection on large-scale flow. *J. Atmos. Sci.*, **31**, 1232–1240.

Lau, K.-M., T. Nakazawa, and C.-H. Sui, 1991: Observations of cloud cluster hierarchy over the tropical western Pacific. *J. Geophys. Res.* **96**, 3197–3208.

Lau, K.-M., C.-H. Sui, and W.-K. Tao, 1993: A preliminary study of the tropical water cycle using the Goddard Cumulus Ensemble model. *Bull. Amer. Meteor. Soc.* **74**, 1313–1321.

Lau, K.-M., C.-H. Sui, M.-D. Chou, and W.-K. Tao, 1994a: An inquiry into the cirrus-cloud thermostat effect for tropical sea surface temperature. *Geophys. Res. Lett.*, **21**, 1157–1160.

Lau, K.-M., C.-H. Sui, M.-D. Chou, and W.-K. Tao, 1994b: Reply to the comment on the paper "An inquiry into the cirrus-cloud thermostat effect for tropical sea surface temperature," by V. Ramanathan, W. D. Collins, and B. Subasilar. *Geophys. Res. Lett.*, **21**, 1187–1188.

Lau, K.-M., and C.-H Sui, 1997: Mechanisms of short-term sea surface temperature regulation: observations during TOGA COARE. *J. Climate*, **10**, 465–472.

Lau, K. M., and H. T. Wu, 2003: Warm rain over tropical oceans and climate implications. *Geophys. Res. Lett.*, **30**, doi:10.1029/ 2003GL018567.

Lau, K. M., H. T. Wu, Y. C. Sud, and G. K. Walker, 2005: Effects of cloud microphysics on tropical atmospheric hydrologic processes and intraseasonal variability in the GEOS GCM, *J. Climate*, **18**, 4731–4751.

Liang, X.-Z., and X. Wu, 2005: Evaluation of a GCM subgrid cloud–radiation interaction parametrization using cloud-resolving model simulations. *Geophys. Res. Lett.*, **32**, L06801, doi:10.1029/2004GL022301.

Li, X., C.-H. Sui, D. Adamec, and K.-M. Lau, 1998: Impacts of precipitation in the upper ocean in the western Pacific warm pool during TOGA COARE. *J. Geophys. Res.*, **103**, C3, 5347–5359.

Li, X., C.-H. Sui, K.-M. Lau, and M.-D. Chou, 1999: Large-scale forcing and cloud–radiation interaction in the tropical deep convective regime. *J. Atmos. Sci.*, **56**, 3028–3042.

Li, X., C.-H. Sui, K.-M. Lau, and D. Adamec, 2000: Effects of precipitation on ocean mixed-layer temperature and salinity as simulated in a 2-D coupled ocean–cloud-resolving atmosphere model. *J. Meteor. Soc. Japan*, **78**, 647–659.

Li, X., C.-H. Sui, and K.-M. Lau, 2002a: Precipitation efficiency in the tropical deep convective regime: a 2-D cloud-resolving modeling study. *J. Meteor. Soc. Japan*, **80**, 205–212.

Li, X., C.-H. Sui, and K.-M. Lau, 2002b: Interactions between tropical convection and its environment: an energetics analysis of a 2-D cloud resolving simulation. *J. Atmos. Sci.*, **59**, 1712–1722.

Li, X., C.-H. Sui, and K.-M. Lau, 2002c: Dominant cloud-microphysical processes in a tropical oceanic convective system: a 2-D cloud resolving modeling study. *Mon. Wea. Rev.*, **130**, 2481–2491.

Li, X., C.-H. Sui, K.-M. Lau, and W.-K. Tao, 2005: Tropical convective responses to microphysical and radiative processes: a sensitivity study with a 2D cloud-resolving modeling study. *Meteor. Atmos. Phys.*, **90**, 245–259.

Lin, S.-J., 2004: A "vertically Lagrangian" finite-volume dynamical core for global models. *Mon. Wea. Rev.*, **132**, 2293–2307.

Lin Y. L., R. D. Farley, and H. D. Orville, 1983: Bulk parametrization of the snow field in a cloud model. *J. Climate Appl. Meteor.*, **22**, 1065–1092.

Lipps, F. B., and R. S. Hemler, 1986: Numerical simulation of deep tropical convection associated with large-scale convergence. *J. Atmos. Sci.*, **43**, 1796–1816.

Lindzen, R. S., 1990: Some coolness concerning global warming. *Bull. Amer. Meteor. Soc.*, **71**, 288–299.

Lindzen, R. S., M. D. Chou, and A. Hou, 2001: Does the earth have an adaptive infrared Iris? *Bull. Am. Meteor. Soc.*, **82**, 417–432.

Lorenz, E. N., 1955: Available potential energy and the maintenance of the general circulation. *Tellus*, **7**, 157–167.

Lukas, R., and E. Lindstrom, 1991: The mixed layer of the western equatorial Pacific Ocean. *J. Geophys. Res.*, **96**, 3343–3457.

Mapes, B. E., 1993: Gregarious tropical convection. *J. Atmos. Sci.*, **50**, 2026–2037.

Mapes, B. E., and R. A. Houze, Jr., 1993: Cloud clusters and superclusters over the oceanic warm pool. *Mon. Wea. Rev.*, **121**, 1398–1415.

Miura, H., H. Tomita, T. Nasuno1, S. Iga1, M. Satoh, and T. Matsuno, 2005: A climate sensitivity test using a global Cloud Resolving Model under an aqua planet condition. *Geophys. Res. Lett.*, **32**, L19719, dot:10.1029/2005GL023672.

Newell, R. E., 1979: Climate and the ocean. *Amer. Sci.*, **67**, 405–416.

Niiler, P. P., and E. B. Kraus, 1977: One-dimensional models. In *Modeling and Prediction of the Upper Layers of the Ocean*, E. B. Kraus (ed.), Pergamon, New York, pp. 143–172.

Orville, H. D., and F. J. Kopp, 1977: Numerical simulation of the life history of a hailstorm. *J. Atmos. Sci.*, **34**, 1596–1618.

Peng, L., C.-H. Sui, K.-M. Lau, and W.-K. Tao, 2001: Genesis and evolution of hierarchical cloud clusters in a two-dimensional cumulus-resolving model. *J. Atmos. Sci.*, **58**, 877–895.

Prabhakara, C., D. P. Kratz, J.-M. Yoo, G. Dalu, and A. Vernekar, 1993: Optically thin cirrus clouds: radiative impact on the warm pool. *J. Quant. Spectrosc. Radiat. Transfer.*, **49**, 467–483.

Ramanathan, V., and W. Collins, 1991: Thermodynamic regulation of ocean warming by cirrus clouds deduced from observations of the 1987 El Niño. *Nature*, **351**, 27–32.

Ramanathan, V., W. D. Collins, and B. Subasilar, 1994: Comments on the paper "An inquiry into the cirrus-cloud thermostat effect for tropical sea surface temperature." *Geophys. Res. Lett.*, **21**, 1185–1186.

Randall, D. A., and D.-M. Pan, 1993: Implementation of the Arakawa–Schubert cumulus parametrization with a prognostic closure. In *The Representation of Cumulus Convection in Numerical Models of the Atmosphere*, K. A. Emanuel and D. J. Raymond, (eds.) *Meteor. Monogr.*, No. 46, pp. 37–144.

Randall, D. A., Harshvardhan and D. A. Dazlich, 1991: Diurnal variability of the hydrologic cycle in a general circulation model. *J. Atmos. Sci.*, **48**, 40–62.

Randall, D. A., M. Khairoutdinov, A. Arakawa, and W. Grabowski, 2003: Breaking the cloud parametrization deadlock.*Bull. Amer. Meteor. Soc.*, 1547–1564.

Rutledge, S. A., and R. V. Hobbs, 1983: The mesoscale and microscale structure and organization of clouds and precipitation in midlatitude cyclones. Part VIII: A model for the "seeder–feeder" process in warm-frontal rainbands. *J. Atmos. Sci.*, **40**, 1185–1206.

Rutledge, S. A., and R. V. Hobbs, 1984: The mesoscale and microscale structure and organization of clouds and precipitation in midlatitude cyclones. Part XII: A diagnostic modeling study of precipitation development in narrow cold-frontal rainbands. *J. Atmos. Sci.*, **41**, 2949–2972.

Satoh, M., H. Tomita, H. Miura, S. Iga, and T. Nasuno, 2005: Development of a global cloud resolving model — a multi-scale structure of tropical convections. *J. Earth Simulator*, **3**, 1–9.

Simpson, J., R. Adler, and G. North, 1988: A proposed Tropical Rainfall Measuring Mission

(TRMM) satellite. *Bull. Amer. Meteor. Soc.*, **69**, 278–295.

Soden, B. J., 1997: Variations in the tropical greenhouse effect during El Niño. *J. Climate*, **10**, 1050–1055.

Soong, S. T., and Y. Ogura, 1980a: Response of tradewind cumuli to large-scale processes. *J. Atmos. Sci.*, **37**, 2035–2050.

Soong, S. T., and W. K. Tao, 1980b: Response of deep tropical cumulus clouds to mesoscale processes. *J. Atmos. Sci.*, **37**, 2016–2034.

Sud, Y. C., and G. K. Walker, 1999: Microphysics of clouds with the relaxed Arakawa–Schubert cumulus scheme (McRAS); Part I: Design and evaluation with GATE Phase III data.*J. Atmos. Sci.*, **56**, 3196–3220.

Sud, Y. C., and G. K. Walker, 2003: Influence of ice-phase physics of hydrometeors on moist convection. *Geophys. Res. Lett.* **30**, 14, 1758–1761.

Sui, C.-H., K.-M. Lau, and A. K. Betts, 1991: An equilibrium Model for the coupled ocean–atmosphere boundary layer in the tropics. *J. Geophys. Res.*, **96**, 3151–3163.

Sui, C.-H., and K.-M. Lau, 1992: Multi-scale phenomena in the tropical atmosphere over the western Pacific. *Mon Wea. Rev.*, **120**, 407–430.

Sui, C.-H., K.-M. Lau, W.-K. Tao, and J. Simpson, 1994: The tropical water and energy cycles in a cumulus ensemble model. Part I: Equilibrium climate. *J. Atmos. Sci.*, **51**, 711–728.

Sui, C.-H., K.-M. Lau, Y. Takayabu, and D. Short, 1997a: Diurnal variations in tropical oceanic cumulus ensemble during TOGA COARE. *J. Atmos. Sci.*, **54**, 639–655.

Sui, C.-H., X. Li, K.-M. Lau, and D. Adamec, 1997b: Multi-scale air–sea interactions during TOGA COARE. *Mon. Wea. Rev.*, **125**, 448–462.

Sui, C.-H., X. Li, and K.-M. Lau, 1998a: Radiative–convective processes in simulated diurnal variations of tropical oceanic convection. *J. Atmos. Sci.*, **55**, 2345–2359.

Sui, C.-H., X. Li, and K.-M. Lau, 1998b: Selective absorption of solar radiation and upper ocean temperature in the equatorial western Pacific. *J. Geophys. Res.*, **103**, C5, 10313–10321.

Sui, C.-H., X. Li, M. M. Rienecker, K.-M. Lau, I. Laszlo, and R. T. Pinker, 2003: The impacts of daily surface forcing in the upper ocean over tropical Pacific: a numerical study. *J. Climate*, **16**, 756–766.

Sui, C.-H., and Li, X., 2005: A tendency of cloud ratio associated with the development of tropical water and ice clouds. *Terr. Atmos. Oceanic Sci.*, **16**, 419–434.

Sui, C.-H., X. Li, M.-J. Yang, and H.-L. Huang, 2005: Estimation of oceanic precipitation efficiency in cloud models. *J. Atmos. Sci.*, **62**, 4358–4370.

Sui, C.-H., C.-T. Tsay, and X. Li, 2007a: Convective–stratiform rainfall separation by cloud content. *J. Geophys. Res.* **112**, D14213, doi:10.1029/2006JD008082.

Sui, C.-H., X. Li, and M.-J. Yang, 2007b: On the definition of precipitation efficiency. *J. Atmos. Sci.*, **64**, 4506–4513.

Sundqvist, H., 1988: Parameterization of condensation and associated clouds in models from weather prediction and general circulation simulation. In *Physical Based Modeling and Simulation of Climate and Climate Change*, M. E. Schlesinger (ed.), Reidel, pp. 433–461.

Sundqvist, H., 1978: A parametrization of non-convective condensation including prediction of cloud water content. *Quart. J. Roy. Meteor. Soc.*, **104**, 677–690.

Tao, W.-K, 2003: Goddard Cumulus Ensemble (GCE) model: application for understanding precipitation processes. In *Cloud Systems, Hurricanes, and the Tropical Rainfall Measuring Mission (TRMM): A Tribute to Dr Joanne Simpson, Meteor. Monogr.,* No. 51, *Amer. Meteor. Soc.*, pp. 107–138.

Tao, W.-K., and J. Simpson, 1984: Cloud interactions and merging: numerical simulations. *J. Atmos. Sci.*, **41**, 2901–2917.

Tao, W.-K., and S.-T. Soong, 1986: The study of the response of deep tropical clouds to mesoscale processes: three-dimensional numerical experiments. *J. Atmos. Sci.*, **43**, 2653–2676.

Tao, W.-K., and J. Simpson, 1989: A further study of cumulus interactions and merging: three-dimensional simulations with trajectory analyses. *J. Atmos. Sci.*, **46**, 2974–3004.

Tao, W.-K., and J. Simpson, 1993: The Goddard cumulus ensemble model. Part I: Model description. *Terr., Atmos. Oceanic Sci.*, **4**, 35–72.

Tao, W.-K., J. Simpson, and M. McCumber, 1989: An ice-water saturation adjustment. *Mon. Wea. Rev.*, **117**, 231–235.

Tao, W.-K., S. Lang, J. Simpson, C.-H. Sui, B. S. Ferrier, and M.-D. Chou, 1996: Mechanisms of

cloud–radiation interaction in the tropics and midlatitude. *J. Atmos. Sci.*, **53**, 2624–2651.

Tao, W.-K., J. Simpson, D. Baker, S. Braun, M.-D. Chou, B. Ferrier, D. Johnson, A. Khain, B. Lynn, S. Lang, C.-L. Shie, C.-H. Sui, Y. Wang, and P. Wetzel, 2003: Microphysics, radiation, and surface processes in a non-hydrostatic model. *Meteor. Atmos. Phys.*, **82**, 97–137.

Tao, W.-K., D. Johnson, C.-L. Shie, and J. Simpson, 2004: The atmospheric energy budget and large-scale precipitation efficiency of convective systems during TOGA COARE, GATE, SCSMEX, and ARM: cloud-resolving model simulations. *J. Atmos. Sci.*, **61**, 2405–2423.

Tiedtke, M., 1993: Representation of clouds in large scale models. *Mon. Wea. Rev.*, **121**, 3040–3061.

Tomita, H., H. Miura, S. Iga, T. Nasuno, and M. Satoh, 2005: A global cloud-resolving simulation: preliminary results from an aqua planet experiment, *Geophys. Res. Lett.*, **32**, L08805, doi:10.1029/2005GL022459.

Thompson, R. M., Jr., S. W. Payne, E. E. Recker, and R. J. Reed, 1979: Structure and properties of synoptic-scale wave disturbances in the intertropical convergence zone of the eastern Atlantic. *J. Atmos. Sci.*, **36**, 53–72.

Vialard, J., and P. Delecluse, 1998a: An OGCM study for the TOGA decade. Part I: Role of salinity in the physics of the western Pacific fresh pool. *J. Phys. Oceanog.*, **28**, 1071–1088.

Vialard, J., and P. Delecluse, 1998b: An OGCM study for the TOGA decade. Part II: Barrier layer formation and variability. *J. Phys. Oceanog.*, **28**, 1089–1106.

Wang, J., and D. A. Randall, 1994: The moist available energy of a conditionally unstable atmosphere. Part II: Further analysis of GATE data. *J. Atmos. Sci.*, **51**, 703–710.

Weisman, M. L., and J. B. Klemp, 1982: The dependence of numerically simulated convective storms on vertical wind shear and buoyancy. *Mon. Wea. Rev.*, **110**, 504–520.

Wu, X., and X.-Z. Liang, 2005: Effect of subgrid cloud–radiation interaction on climate simulations. *Geophys. Res. Lett.*, **32**, L06801, doi:10.1029/2004GL022301.

Wu, X., and M. W. Moncrieff, 2001: Long-term behavior of cloud systems in TOGA COARE and their interactions with radiative and surface processes. Part III: Effects on the energy budget and SST. *J. Atmos. Sci.*, **58**, 1155–1168.

Wu, X., X.-Z. Liang, G.-J., Zhang 2003: Seasonal migration of ITCZ precipitation across the equator: Why can't GCMs simulate it? *Geophys. Res. Lett.*, **30**, 1824, doi:10.1029/2003GL017198.

Wu, X., W. W. Grabowski, and M. W. Moncrieff, 1998: Long-term evolution of cloud systems in TOGA COARE and their interactions with radiative and surface processes. Part I: Two-dimensional cloud-resolving model. *J. Atmos. Sci.*, **55**, 2693–2714.

Xu, K.-M., and D. A. Randall, 1995: Impact of interactive radiative transfer on the macroscopic behavior of cumulus ensembles. Part II: Mechanisms for cloud–radiation interactions. *J. Atmos. Sci.,* **52,** 800–817.

Xu, K.-M., and D. A. Randall, 1996: Explicit simulation of cumulus ensembles with the GATE Phase III data: comparison with observations. *J. Atmos. Sci.*, **53**, 3710–3736.

Xu, K.-M., and D. A. Randall, 1998: Influence of large-scale advective cooling and moistening effects on the quasi-equilibrium behavior of explicitly simulated cumulus ensembles. *J. Atmos. Sci.*, **55**, 896–909.

Yanai, M., S. Esbensen, and J.-H. Chu, 1973: Determination of bulk properties of tropical cloud clusters from large-scale heat and moisture budgets. *J. Atmos. Sci.*, **30**, 611–627.

Yang, M.-J., and H.-L. Huang, 2004: Precipitation processes associated with the landfalling Typhoon Nari (2001). In *Preprints, The 26th Conference on Hurricanes and Tropical Meteorology*, Miami, 3–7 May 2004, *Amer. Meteor. Soc.*, pp. 134–135.

Zhang, G.-J., and X. Wu, 2003: Convective momentum transport and perturbation pressure field from a cloud-resolving model simulation. *J. Atmos. Sci.*, **60**, 1120–1139.

Zhang, M. H., R. D. Cess, and S. C. Xie, 1996: Relationship between cloud radiative forcing and sea surface temperatures over the entire tropical oceans. *J. Climate*, **9**, 1374–1384.

Zhao, Q., and F. H. Carr, 1997: A prognostic cloud scheme for operational NWP models. *Mon. Wea. Rev.*, **125**, 1931–1953.